J Therm Anal Calorim (2014) 118:1577–1584
DOI 10.1007/s10973-014-4068-9

An experimental study on thermal decomposition behavior of magnesite

Lu Tian · Arash Tahmasebi · Jianglong Yu

Received: 5 May 2014 / Accepted: 3 August 2014 / Published online: 29 August 2014

Abstract Thermal decomposition of magnesite is investigated by using a TG–MS. Different kinetic methods including Coats–Redfern, Flynn–Wall–Ozawa, and Kissinger–Akahira–Sunose are used to investigate the thermal decomposition kinetics of magnesite. It was observed that the activation energy values obtained by these methods are similar. The average apparent activation energy is found to be about 203 kJ mol^{-1}. The raw magnesite and its decomposition products obtained at different temperatures are analyzed by Fourier transform infrared spectroscopy (FTIR), X-ray diffraction (XRD), and scanning electron microscope (SEM). The concentration of functional groups, crystal structure and composition, and apparent morphology of decomposition products were studied in detail. The FTIR, XRD, and SEM analyses showed that magnesite was completely decomposed at 973 K to form MgO.

Keywords Magnesite · Thermal decomposition · Thermogravimetric analysis · Activation energy

Introduction

China is one of the richest countries in magnesite ($MgCO_3$) resources which account for one third of world magnesite production [1]. Liaoning province is the richest area in magnesite reserves in China with 3.4 billion tons of proved reserves [2]. Magnesite is usually calcined to produce magnesium oxide (MgO) which is used as refractory materials. Magnesite is considered as one of the most important refractory raw materials because of its high fire resistance. Magnesium hydrate made from MgO is used as an absorbent in wet flue gas desulfurization [3, 4]. Magnesite is also used as building materials and chemical raw materials, and in elemental magnesium production as well as in the production of other magnesium compounds [2]. A more efficient use of magnesite requires a better understanding of its decomposition characteristics.

Recently, a number of studies on decomposition of magnesite have been reported in the literature [5–8]. Thermal decomposition of magnesite is studied by Liu et al. [5]. They reported the activation energy (E) and pre-exponential factor ($\log A$) of 156.12 kJ mol^{-1} and 105.61 s^{-1}, respectively. Demir et al. [6] investigated the thermal decomposition kinetics of magnesite by using Coats–Redfern and Suzuki methods, and reported that a first-order kinetic model best described the decomposition reaction. They also studied the effect of particle size on reaction kinetics and reported that activation energy decreased with decreasing particle size and varied between 236 and 302 kJ mol^{-1}. Hurst [7] investigated the decomposition of two particle size fractions of magnesite by non-isothermal thermogravimetric analysis and reported that contracting core model (R3) can describe the decomposition of magnesite with highest accuracy. He reported the values of 161 kJ mol^{-1} and 2.9×10^8 min^{-1} for the activation energy and pre-exponential constant, respectively. Sheila [8] investigated the decomposition kinetics of magnesite as a function of temperature and particle size, and found that the diffusion model fits best to experimental data and the activation energy is in the range of 95–104 kJ mol^{-1}.

L. Tian · A. Tahmasebi · J. Yu (✉)
Key Laboratory of Advanced Coal and Coking Technology of Liaoning Province, School of Chemical Engineering, University of Science and Technology Liaoning, Anshan 114051, People's Republic of China
e-mail: jianglong.yu@newcastle.edu.au

J. Yu
Chemical Engineering, University of Newcastle, Callaghan, NSW 2308, Australia

Apart from thermogravimetric analysis, the decomposition behavior of inorganic materials can also be investigated by X-ray diffraction (XRD), Fourier transform infrared spectroscopy (FTIR), and scanning electron microscopy (SEM). Unluer [9] studied the thermal decomposition of hydrated magnesium carbonates and investigated the properties of various products by using SEM, XRD, and TG. Hu et al. [10] studied thermal decomposition of $ZnC_2O_4{\cdot}2H_2O$, and used FTIR and XRD to characterize the decomposition products. They used Ozawa and Coats–Redfern integral methods to determine the kinetic parameters of the thermal decomposition of $ZnC_2O_4{\cdot}2H_2O$.

In this paper, non-isothermal decomposition behavior of magnesite is studied using a TG-MS. Three methods namely Coats–Redfern, Flynn–Wall–Ozawa (FWO), and Kissinger–Akahira–Sunose (KAS) are used to calculate the kinetics parameters. Properties of decomposition products such as concentration of function groups, crystal structure, composition, and morphology are analyzed by FTIR, XRD, and SEM.

Experimental and methodology

Materials

Magnesite used in the work was obtained from Haicheng region in Liaoning Province, China. The chemical compositions of the sample measured by X-ray fluorescence (XRF) are as follows: 47.1 % MgO, 0.276 % CaO, 0.757 % Fe_2O_3, 0.038 % Al_2O_3, 0.144 % SiO_2, and 51.72 % ignition loss. The magnesite ore was crushed and sieved to a particle size of less than 0.5 mm.

Thermogravimetric analysis

Non-isothermal decomposition experiments were carried out by using TG-MS (NETZSCH STA 449 F3 coupled with NETZSCH QMS 403 C). About 10 mg of sample with a particle size of less than 0.74 μm was loaded into Pt crucible, and the mass loss and gaseous products evolution were recorded by TG and MS, respectively. Samples were heated in the temperature range between 303 and 1,173 K with heating rates of 2, 5, 10, and 15 K min^{-1} under N_2 gas flow of 80 mL min^{-1}. Coats–Redfern, FWO, and KAS methods were applied to investigate the thermal decomposition kinetics of magnesite.

Calculation of kinetic parameters using different models

The decomposition reaction of magnesite is a typical solid-state decomposition reaction. The conversion of magnesite can be written as [11]:

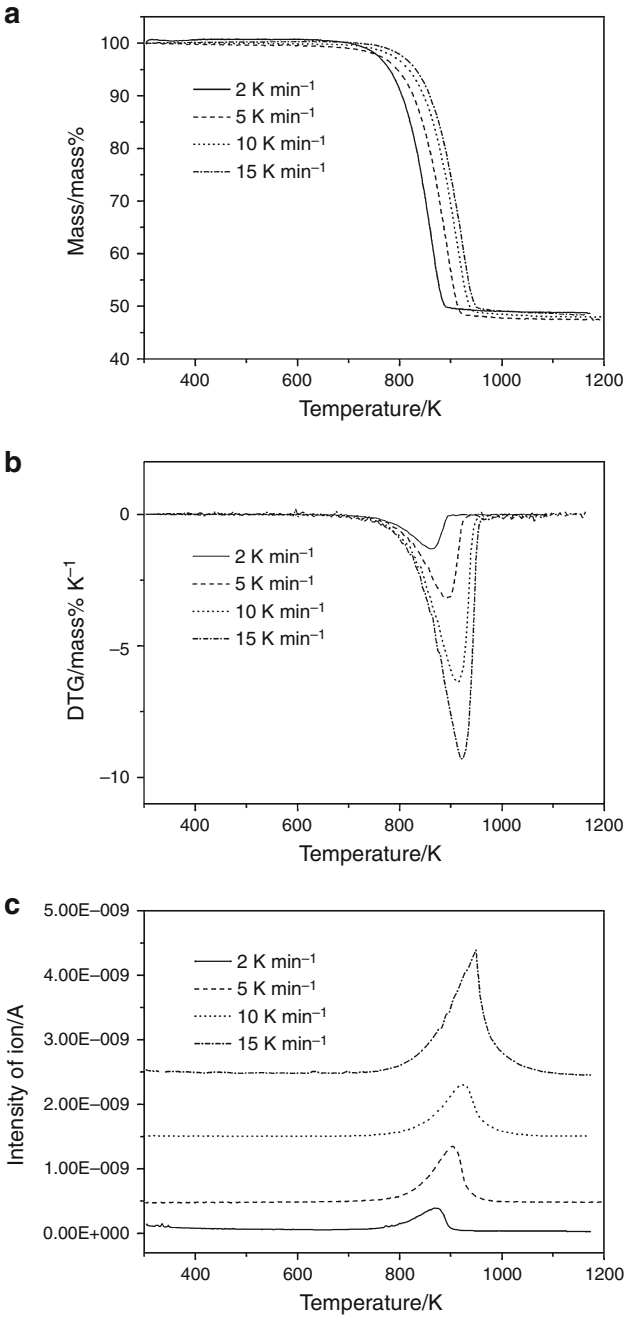

Fig. 1 TG, DTG, and CO_2 evolution curves on the thermal decomposition of magnesite at different heating rates: **a** TG; **b** DTG; **c** CO_2 evolution

$$\alpha = \frac{m_0 - m_t}{m_0 - m_\infty}, \quad (1)$$

where α is the conversion, m_0 is the initial mass of magnesite, m_t is the mass at time t, and m_∞ is the final mass of the sample after the reaction.

In the non-isothermal experiments, the sample mass is recorded as a function of the temperature. According to non-isothermal kinetic theory, the isoconversional method

Table 1 Activation energy and correlation coefficients calculated by FWO and KAS methods at different conversions

α	FWO		KAS	
	R^2	E/kJ mol^{-1}	R^2	E/kJ mol^{-1}
0.2	0.9988	200.58276	0.9987	197.09752
0.3	0.9984	203.09839	0.9983	199.46921
0.4	0.9962	205.70746	0.9958	202.00428
0.5	0.9913	207.02658	0.9902	203.22417
0.6	0.9900	207.85466	0.9889	203.94242
0.7	0.9873	209.33472	0.9857	205.36112
0.8	0.9857	210.98965	0.9838	206.96601

can be applied to a solid-state reaction. The rate of conversion under linear temperature increasing condition can be generally described as [12, 13]:

$$\frac{d\alpha}{dt} = k(T)f(\alpha), \tag{2}$$

where t is the time, T is the temperature, $k(T)$ is the temperature-dependent rate constant, and $f(\alpha)$ is the temperature-independent function of conversion. The reaction rate constant according to Arrhenius equation, $k(T)$, can be written as:

$$k(T) = A\exp\left(\frac{-E}{RT}\right), \tag{3}$$

where A is the pre-exponential factor, E is the activation energy, R is the universal gas constant, and β is the heating rate. The kinetic equation can therefore be expressed as [14]:

$$\frac{d\alpha}{dt} = \beta\frac{d\alpha}{dt} = k(T)f(\alpha) = A\exp\left(\frac{-E}{RT}\right)f(\alpha). \tag{4}$$

It has been reported that the isoconversional method is the most common method to calculate the activation energy independent of the reaction mechanism [15]. Unlike conventional isothermal method, the isoconversional method has the advantage of calculation of the activation energy without prior knowledge of the $f(\alpha)$ function [14, 16]. In this study, FWO [17, 18] and KAS [19] methods are used to calculate the activation energy [20]. Different heating rates are used in the kinetic analysis to obtain the apparent activation energy via FWO and KAS methods [14, 21].

The FWO method is based on the following equation:

$$\ln\beta = \ln\frac{0.0084AE}{g(\alpha)R} - 1.0516\frac{E}{RT}. \tag{5}$$

The KAS method can be described by the following equation [11]:

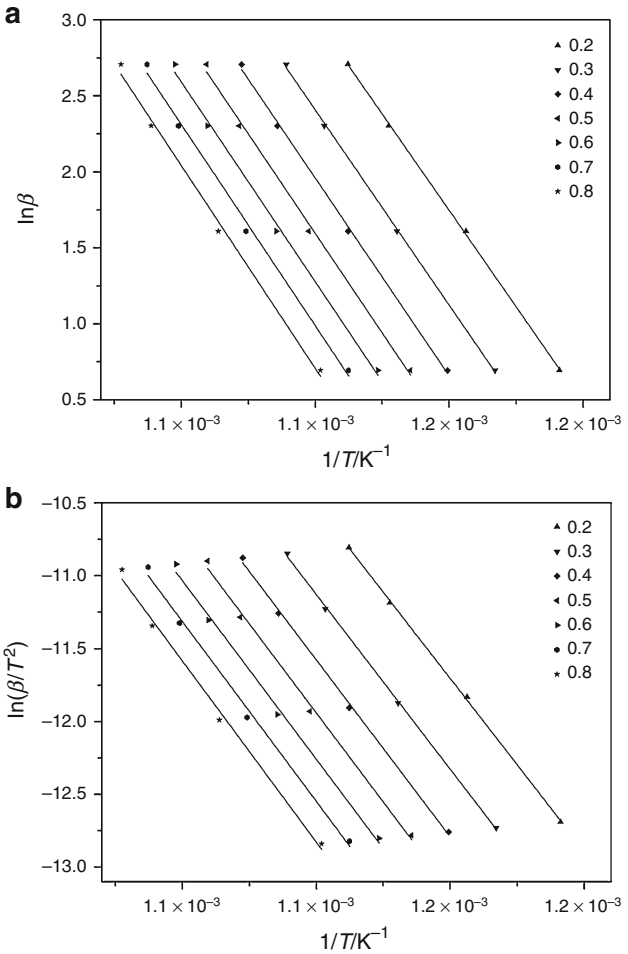

Fig. 2 Plots for determination of activation energy and pre-exponential factor by: **a** FWO method; **b** KAS method

$$\ln\frac{\beta}{T^2} = \ln\frac{AR}{g(\alpha)E} - \frac{E}{RT}. \tag{6}$$

For α = const., the plots between $\ln(\beta)$ versus $1/T$ and $\ln(\beta/T^2)$ versus $1/T$ yield straight lines whose slope allows evaluation of the apparent activation energy.

The Coats–Redfern method is also alternatively used to calculate the kinetic parameters and to determine the reaction order and mechanism [22, 23]. Coats–Redfern equation can be expressed as follows [23]:

$$\ln\left[\frac{g(\alpha)}{T^2}\right] = \ln\frac{k_0R}{qE} - \frac{E}{RT}, \tag{7}$$

$$q = \frac{dT}{dt}, \tag{8}$$

where k_0 is the frequency factor. The plot of $\ln[g(\alpha)/T^2)$ versus $1/T$ yields a straight line whose slope allows evaluation of the apparent activation energy.

Table 2 Mathematical models for the most common solid-state reaction mechanisms [26, 27]

No.	Mechanism	Function name	Differential form $f(\alpha)$	Integral form $g(\alpha)$
1	F0.6	Chemical reaction, $n = 0.6$	$1/0.6(1-\alpha)[-\ln(1-\alpha)]^{0.4}$	$1-\ln(1-\alpha)^{0.4}$
2	F0.7	Chemical reaction, $n = 0.7$	$1/0.7(1-\alpha)[-\ln(1-\alpha)]^{0.3}$	$1-\ln(1-\alpha)^{0.3}$
3	F0.8	Chemical reaction, $n = 0.8$	$1/0.8(1-\alpha)[-\ln(1-\alpha)]^{0.2}$	$1-\ln(1-\alpha)^{0.2}$
4	F0.9	Chemical reaction, $n = 0.9$	$1/0.9(1-\alpha)[-\ln(1-\alpha)]^{0.1}$	$1-\ln(1-\alpha)^{0.1}$
5	F1	Chemical reaction, $n = 1$	$1-\alpha$	$-\ln(1-\alpha)$
6	F1.1	Chemical reaction, $n = 1.1$	$1/1.1(1-\alpha)[-\ln(1-\alpha)]^{-0.1}$	$1-\ln(1-\alpha)^{-0.1}$
7	F1.2	Chemical reaction, $n = 1.2$	$1/1.2(1-\alpha)[-\ln(1-\alpha)]^{-0.2}$	$1-\ln(1-\alpha)^{-0.2}$
8	D1 1-D diffusion	Parabola law	$1/(2\alpha)$	α^2
9	D2 2-D diffusion	Valensi equation	$-[\ln(1-\alpha)]^{-1}$	$(1-\alpha)\ln(1-\alpha)+\alpha$
10	D3 3-D diffusion	Jander equation	$3/2\left[1-(1-\alpha)^{1/3}\right]^{-1}(1-\alpha)^{2/3}$	$\left[1-(1-\alpha)^{1/3}\right]^2$
11	D4 4-D diffusion	Ginstling–Brounstein equation	$3/2\left[1-(1-\alpha)^{1/3}\right]^{-1}$	$(1-2\alpha/3)-(1-\alpha)^{2/3}$
12	R2 Phase boundary contracting reaction	Contracting surface	$2(1-\alpha)^{1/2}$	$1-(1-\alpha)^{1/2}$
13	R3 Phase boundary contracting reaction	Contracting volume	$3(1-\alpha)^{2/3}$	$1-(1-\alpha)^{1/3}$
14	A1.5 Random nucleation and nuclei growth	Avrami–Erofeev equation	$3/2(1-\alpha)[-\ln(1-\alpha)]^{1/3}$	$[-\ln(1-\alpha)]^{2/3}$
15	A2 Random nucleation and nuclei growth	Avrami–Erofeev equation	$2(1-\alpha)[-\ln(1-\alpha)]^{1/2}$	$[-\ln(1-\alpha)]^{1/2}$
16	A3 Random nucleation and nuclei growth	Avrami–Erofeev equation	$3(1-\alpha)[-\ln(1-\alpha)]^{2/3}$	$[-\ln(1-\alpha)]^{1/3}$
17	A4 Random nucleation and nuclei growth	Avrami–Erofeev equation	$4(1-\alpha)[-\ln(1-\alpha)]^{3/4}$	$[-\ln(1-\alpha)]^{1/4}$

Analysis of decomposition products

Isothermal decomposition experiments were carried out in a cylindrical fixed-bed quartz reactor with an internal diameter of 20 mm heated by an electric furnace. Samples of 2 g were loaded into the reactor and were heated at 673, 923, and 1,173 K under N_2 for 30 min. The concentration of functional groups, crystal structure and composition, and apparent morphology of raw magnesite and its decomposition products are investigated by FTIR, XRD, and SEM.

Infrared (IR) spectra of samples were obtained by using a Thermo Fisher Nicolet IS5 mid-FTIR spectrometer. KBr pellets were prepared by grinding 1.0 mg of coal sample with 100 mg KBr. The IR spectra of the samples are obtained in the 4,000–400 cm^{-1} region. Prior to FTIR measurements, a reference spectrum is obtained from pure KBr pellets without the addition of any sample.

The crystal structure and composition of magnesite and its decomposition products were analyzed by XRD (Shimadzu X-ray diffractometer-7000). The X-ray pattern of sample was recorded with a step-scanning method in the range of $2\theta = 5°$–$85°$ with the rate of 2°/min. The surface morphology of magnesite and its decomposition products were analyzed by using a SEM (JSM-6480).

Results and discussion

Thermogravimetric analysis results

The TG, DTG, and CO_2 evolution curves for magnesite decomposition at different heating rates (2, 5, 10, and 15 K min^{-1}) are shown in Fig. 1. The decomposition reaction of magnesite is expressed as follows:

$$MgCO_3(s) \rightarrow MgO(s) + CO_2(g). \quad (9)$$

TG curves indicate that the decomposition of magnesite takes place in the temperature range of 673–1,173 K (Fig. 1a). It can be seen that the thermal decomposition of magnesite starts at around 733 K and reaches to its maximum rate in the temperature range of 873–923 K. Magnesite is completely decomposed to MgO at 973 K. Similar results have been reported in the literature [24]. The MS results on CO_2 evolution shown in Fig. 1c are consistent with TG results. With increasing heating rate, TG curves are shifted to higher temperatures. The total mass loss is 51.7 %, which is consistent with the ignition loss of the raw magnesite sample. With increasing heating rate, the maximum mass loss rate (DTG_{max}) increases significantly (Fig. 1b). Similar trend is observed in evolution rate of

CO_2 (Fig. 1c). The single TG and DTG curve indicates that the thermal decomposition of magnesite is a one-step reaction [5, 6].

Kinetics parameters calculated using different kinetic models

The activation energies and correlation coefficients calculated by FWO and KAS methods are listed in Table 1 and regression curves are shown in Fig. 2. As can be seen from Table 1, the correlation coefficients higher than 0.99 in all cases are achieved, showing the high accuracy of the results. The activation energy values calculated from FWO and KAS methods are 206.4 and 202.6 kJ mol^{-1}, respectively. These values are in good agreement with the theoretical values (204 kJ mol^{-1}) reported in the literature [25]. The activation energy of 156.34 kJ mol^{-1} calculated by KAS method for the decomposition of magnesite has also been reported in literature [5]. The difference in activation energy values can be attributed to the difference in the composition of the samples used and calculation methods.

The Coats–Redfern method is also used to determine the kinetic parameters and the mechanism of magnesite reduction. The reaction mechanism and order are predefined in Coats–Redfern method. The integral and differential forms of the mathematical models for common solid-state reaction mechanisms reported in the literature are given in Table 2 [26, 27]. The decomposition mechanism of magnesite in the conversion range of $0.25 < \alpha < 0.95$ is evaluated. The activation energies and correlation coefficients for different reaction mechanisms are calculated by using the Coats–Redfern method and are listed in Table 3. As mentioned above, the value of activation energy calculated by FWO and KAS methods is

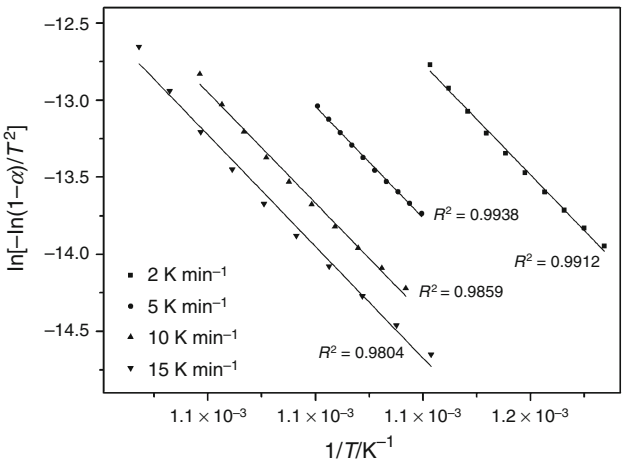

Fig. 3 Linear regression for F1 mechanism at different heating rates by Coats–Redfern method

Table 4 Activation energies for thermal decomposition of magnesite

Method	E/kJ mol^{-1}
Coats–Redfern	199.99
Flynn–Wall–Ozawa	206.37
Kissinger–Akahira–Sunose	202.58
Average	202.98

Table 3 Activation energies and correlation coefficients for different mechanisms by Coats–Redfern method at different heating rates

Mechanism	2 K min^{-1}		5 K min^{-1}		10 K min^{-1}		15 K min^{-1}	
	E/kJ mol^{-1}	R^2	E/kJ mol^{-1}	R^2	E/kJ mol^{-1}	R^2	E/kJ mol^{-1}	R^2
F0.6	152.99	0.9995	152.11	0.9986	154.50	0.9986	158.58	0.9989
F0.7	163.88	0.9984	163.34	0.9977	164.85	0.9966	168.31	0.9963
F0.8	175.33	0.9966	175.13	0.9966	175.72	0.9937	178.57	0.9924
F0.9	187.33	0.9941	187.46	0.9953	187.11	0.9901	189.35	0.9870
F1	199.90	0.9912	200.35	0.9938	199.02	0.9859	200.67	0.9804
F1.1	213.03	0.9879	213.80	0.9923	211.46	0.9811	212.52	0.9727
F1.2	226.73	0.9842	227.80	0.9906	224.42	0.9759	224.90	0.9640
D1	179.02	0.9904	206.14	0.9977	220.24	0.9904	333.78	0.9800
D2	222.58	0.9985	259.81	0.9996	269.63	0.9989	398.63	0.9958
D3	283.16	0.9987	333.85	0.9982	337.71	0.9975	489.14	0.9982
D4	242.37	0.9998	284.06	0.9996	291.88	0.9999	428.09	0.9992
R2	120.70	0.9999	141.41	0.9993	144.65	0.9997	211.64	0.9998
R3	135.55	0.9986	159.54	0.9980	161.34	0.9973	233.87	0.9981
A1.5	108.73	0.9899	128.64	0.9934	127.67	0.9849	182.53	0.9810
A2	78.53	0.9892	92.79	0.9929	91.99	0.9837	131.54	0.9795
A3	48.33	0.9876	56.93	0.9917	56.32	0.9810	80.56	0.9760
A4	33.23	0.9856	39.00	0.9902	38.48	0.9775	55.07	0.9715

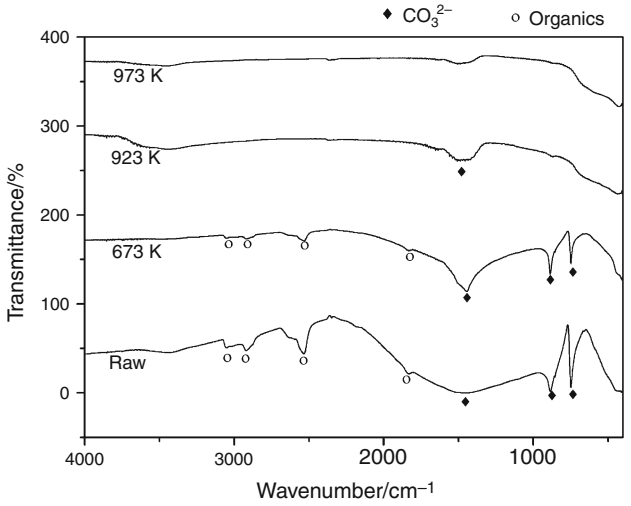

Fig. 4 FTIR spectra on raw magnesite and the solid products after decomposition at different temperatures

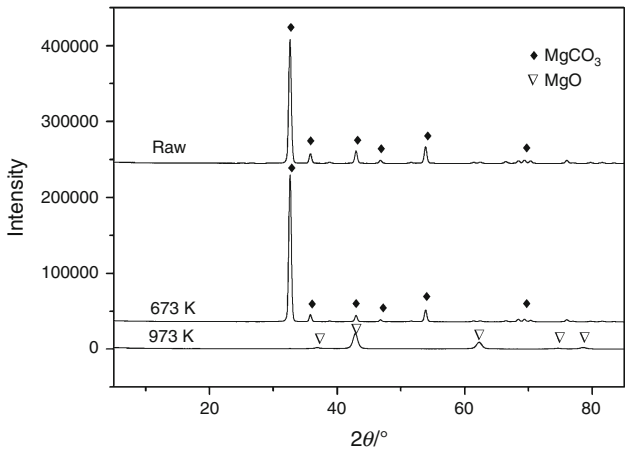

Fig. 5 XRD analysis of raw magnesite and its solid decomposition products

independent of the reaction mechanism. Therefore, the average activation energy of 204.47 kJ mol^{-1} obtained by FWO and KAS methods is considered as the actual value, and the corresponding mechanism to this value in Coats-Redfern method is chosen as the reaction mechanism of magnesite decomposition. The activation energy corresponding to F1 mechanism is in best agreement with the values obtained by FWO and KAS methods. Therefore, it can be concluded that the decomposition of magnesite follows the first-order (F1) chemical reaction mechanism.

The differential ($f(\alpha)$) and integral ($g(\alpha)$) forms of magnesite thermal decomposition can be written as

$$f(\alpha) = (1-\alpha), \tag{10}$$

$$g(\alpha) = -\ln(1-\alpha). \tag{11}$$

The Eq. 7 can therefore be written as

$$\ln\left[\frac{-\ln(1-\alpha)}{T^2}\right] = \ln\frac{k_0 R}{qE} - \frac{E}{RT}. \tag{12}$$

The linear regression for different heating rates calculated by first-order reaction is shown in Fig. 3. As can be seen, a good correlation is obtained by using the first-order chemical reaction. The activation energy E calculated by using the Coats–Redfern, FWO, and KAS methods is summarized in Table 4. The average activation energy for the thermal decomposition of magnesite is in the range of 199.99–206.37 kJ mol^{-1}.

Results of FTIR analysis

FTIR method was used to analyze the chemical structure of magnesite decomposition products at different temperatures. The IR spectra of raw magnesite and its decomposition products at different temperatures are shown in Fig. 4. It can be seen that the raw magnesite has a broad peak at around 3,430 cm^{-1} which is attributed to the presence of small amount of water in the sample. The three peaks at 1440, 882, and 745 cm^{-1} correspond to the vibration of CO_3^{2-} [28]. The peak at 879 cm^{-1} is attributed to out-of-plane CO_3^{2-} bending vibration, and the peak at 742 cm^{-1} corresponds to in-plane CO_3^{2-} vibration [29]. The absorption bands of 3052, 2534, 2920, and 1834 cm^{-1}

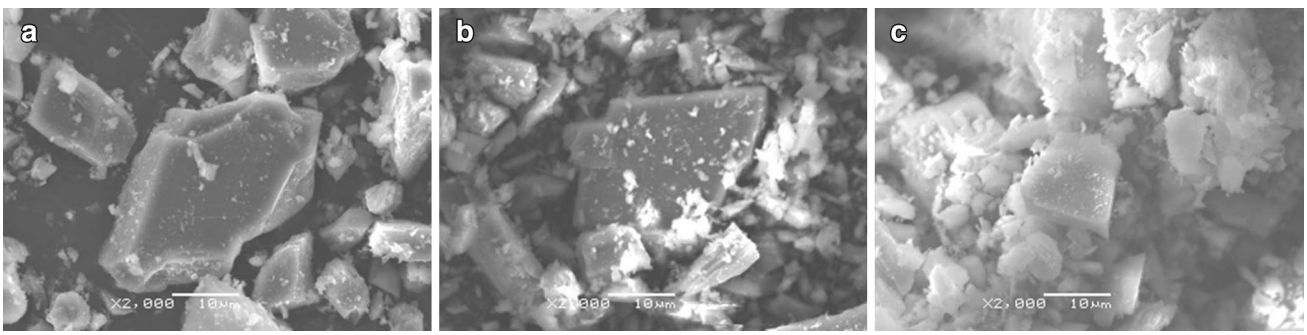

Fig. 6 SEM images of raw magnesite and its solid decomposition products: **a** raw magnesite; **b** decomposed at 673 K; **c** decomposed at 973 K

are assigned to the organic matter in the samples. The IR spectrum of magnesite decomposition product at 673 K shows the disappearance of the peak at 3,430 cm^{-1} as a result of drying. The absorption of CO_3^{2-} and organic functional groups also decreases as a result of partial decomposition of magnesite. The IR spectra of sample after decomposition at 923 K show that organic functional groups are completely decomposed and carbonate adsorption is decreased significantly. After decomposition at 973 K, no carbonate adsorption is detected. It can be concluded that the decomposition of magnesite strongly depends on the temperature and magnesite is completely decomposed to MgO at 973 K.

Results of XRD analysis

The changes in crystalline structure of raw magnesite and its decomposition products as a function of temperature are studied by XRD and the results are given in Fig. 5. As can be seen, the raw magnesite is mainly consisted of $MgCO_3$. After heating at 673 K, little change is observed on the crystalline structure of magnesite. However, after heating at 973 K, magnesite is completely decomposed to form MgO. These results are in agreement with those obtained from FTIR and TG–MS analyses. Raw magnesite has a hexagonal structure, whilst MgO shows trigonal crystalline structure.

Results of SEM analysis

The SEM images of raw magnesite and its decomposition products at 673 and 973 K are shown in Fig. 6. When the decomposition temperature is 673 K, little changes in morphology are observed in the sample compared to its raw form (in Fig. 6b). However, when the decomposition temperature is increased to 973 K, the formation of MgO from decomposition of magnesite and the change in morphology of the sample become rather obvious, as shown in Fig. 6c, with more particles fragmented.

The findings of this study can be used to optimize the production of magnesium oxide for flue gas and coke oven gas (COG) desulfurization purposes. Future study can be focused on desulfurization behavior of MgO produced under different conditions in order to achieve the highest desulfurization efficiency and sulfur capacity.

Conclusions

Thermal decomposition of magnesite starts at 733 K and reaches to the maximum rate in the temperature range of 873–923 K. Magnesite is completely decomposed to MgO at 973 K. The evolution of CO_2 is consistent with the mass loss curves obtained by TG–MS. Thermal decomposition of magnesite follows a first-order chemical reaction mechanism, and the activation energy of magnesite calculated from FWO, KAS, and Coats–Redfern methods is in the range of 199.99–206.37 kJ mol^{-1}.

FTIR analysis showed that with increasing temperature, concentrations of carbonate ions and organic functional groups in magnesite decrease significantly. XRD analysis showed that at 973 K, hexagonal $MgCO_3$ crystals are completely decomposed and form trigonal MgO crystals.

Acknowledgements This study was supported by the Natural Science Foundation of China (21176109, U1361120, and 21210102058). The authors also acknowledge the financial support through the Liaoning Outstanding Professorship Program (2011).

References

1. Ding J, Chen Z, Yang G. Metallogeny and resource potential of magnesite deposits in China. Geol China. 2013;40:1699–711.
2. He Y, Jiang M. Present situation of mining and utilization and existing problems of magnesite resource of our country. Refract Lime. 2012;37(3):25–8.
3. Shen Z, Ni M, Guo S, Chen X, Tong M, Lu J. Studies on magnesium-based wet flue gas desulphurization process with a spray scrubber. Asian J Chem. 2013;25:6727–32.
4. Guo RT, Pan WG, Zhang XB, Jin Q, Xu HJ, Ren JX. The effect of heat decomposition temperature on the dissolution rate of magnesium-based materials for wet flue gas desulfurization. Energy Sour Part A. 2014;36:1–4.
5. Liu X, Feng Y, Li H, Zhang P, Wang P. Thermal decomposition kinetics of magnesite from thermogravimetric data. J Therm Anal Calorim. 2012;107:407–12.
6. Demir F, Dönmez B, Okur H, Sevim F. Calcination kinetic of magnesite from thermogravimetric data. Chem Eng Res Des. 2003;81:618–22.
7. Hurst H. The thermal decomposition of magnesite in nitrogen. Thermochim Acta. 1991;189:91–6.
8. Sheila D. Thermal analysis studies on the decomposition of magnesite. Int J Min Process. 1993;37:73–88.
9. Unluer C, Al-Tabbaa A. Characterization of light and heavy hydrated magnesium carbonates using thermal analysis. J Therm Anal Calorim. 2014;115:595–607.
10. Hu C, Mi J, Shang S, Shangguan J. The study of thermal decomposition kinetics of zinc oxide formation from zinc oxalate dihydrate. J Therm Anal Calorim. 2014;115:1119–25.
11. Ren H, Chen Z, Wu Y, Yang M, Chen J, Hu H, et al. Thermal characterization and kinetic analysis of nesquehonite, hydromagnesite, and brucite, using TG–DTG and DSC techniques. J Therm Anal Calorim. 2014;115:1949–60.
12. Samtani M, Dollimore D, Alexander K. Comparison of dolomite decomposition kinetics with related carbonates and the effect of procedural variables on its kinetic parameters. Thermochim Acta. 2002;392:135–45.
13. Šimon P, Thomas P, Dubaj T, Cibulková Z, Peller A, Veverka M. The mathematical incorrectness of the integral isoconversional methods in case of variable activation energy and the consequences. J Therm Anal Calorim. 2014;115:853–9.
14. Tahmasebi A, Kassim MA, Yu J, Bhattacharya S. Thermogravimetric study of the combustion of *Tetraselmis suecica* microalgae and its blend with a Victorian brown coal in O_2/N_2 and O_2/CO_2 atmospheres. Bioresour Technol. 2013;150:15–27.

15. Meng F, Yu J, Tahmasebi A, Han Y. Pyrolysis and combustion behavior of coal gangue in O_2/CO_2 and O_2/N_2 mixtures using thermogravimetric analysis and a drop tube furnace. Energy Fuels. 2013;27:2923–32.
16. Ledeţi I, Fuliaş A, Vlase G, Vlase T, Bercean V, Doca N. Thermal behaviour and kinetic study of some triazoles as potential anti-inflammatory agents. J Therm Anal Calorim. 2013;114:1295–305.
17. Flynn JH, Wall LA. A quick, direct method for the determination of activation energy from thermogravimetric data. J Polym Sci. 1966;4:323–8.
18. Ozawa T. A new method of analyzing thermogravimetric data. Bull Chem Soc Jpn. 1965;38:1881–6.
19. Kissinger HE. Reaction kinetics in differential thermal analysis. Anal Chem. 1957;29:1702–6.
20. Çılgı G, Koyundereli CH, Donat R. Thermal and kinetic analysis of uranium salts. J Therm Anal Calorim. 2014;108:1213–22.
21. Muraleedharan K. Thermal decomposition kinetics of potassium iodate. J Therm Anal Calorim. 2013;114:491–6.
22. Yilmaz MS, Figen AK, Pişkin S. Study on the dehydration kinetics of tunellite using non-isothermal methods. Res Chem Intermed. 2013. doi:10.1007/s11164-013-1318-6.
23. Coats AW, Redfern JP. Kinetic parameters from thermogravimetric data. Nature. 1964;201:68–9.
24. Pilarska A, Paukszta D, Szwarc K, Jesionowski T. The effect of modifiers and precipitation conditions on physicochemical properties of $MgCO_3$ and its calcinates. Physicochem Problem Min Process. 2011;46:79–90.
25. L'vov BV. Mechanism and kinetics of thermal decomposition of carbonates. Thermochim Acta. 2002;386:1–16.
26. Trittschack R, Grobéty B, Brodard P. Kinetics of the chrysotile and brucite dehydroxylation reaction: a combined non-isothermal/isothermal thermogravimetric analysis and high-temperature X-ray powder diffraction study. Phys Chem Miner. 2014;41:198–214.
27. Jia C, Wang Q, Ge J, Xu X. Pyrolysis and combustion model of oil sands from non-isothermal thermogravimetric analysis data. J Therm Anal Calorim. 2014;116:1073–81.
28. Yang N, Yue W. Inorganic non-metallic materials atlas manual. Wuhan university of technology press; 2000.
29. Lijiang W. Non-metallic mineral processing technology foundation. Beijing: Chemical Industry Press; 2010.